Direct evidence of a zigzag spin-chain structure in the honeycomb lattice: A neutron and x-ray diffraction investigation of single-crystal Na_{2}IrO_{3}

Feng Ye, Songxue Chi, Huibo Cao, Bryan C. Chakoumakos, Jaime A. Fernandez-Baca, Radu Custelcean, T. F. Qi, O. B. Korneta, and G. Cao

Phys. Rev. B **85**, 180403 — Published 8 May 2012

DOI: 10.1103/PhysRevB.85.180403

Direct evidence of a zigzag spin chain structure in the honeycomb lattice: A neutron and x-ray diffraction investigation of single crystal Na_2IrO_3

Feng Ye,[1] Songxue Chi,[1] Huibo Cao,[1] Bryan C. Chakoumakos,[1]
Jaime A. Fernandez-Baca,[1,2] Radu Custelcean,[3] T. F. Qi,[4] O. B. Korneta,[4] and G. Cao[4]

[1] *Quantum Condensed Matter Division, Oak Ridge National Laboratory, Oak Ridge, Tennessee 37831, USA*
[2] *Department of Physics and Astronomy, University of Tennessee, Knoxville, Tennessee 37996, USA*
[3] *Chemical Science Division, Oak Ridge National Laboratory, Oak Ridge, Tennessee 37831, USA*
[4] *Center for Advanced Materials, Department of Physics and Astronomy, University of Kentucky, Lexington, Kentucky 40506, USA*

(Dated: April 30, 2012)

We have combined single crystal neutron and x-ray diffractions to investigate the magnetic and crystal structures of the honeycomb lattice Na_2IrO_3. The system orders magnetically below 18.1(2) K with Ir^{4+} ions forming zigzag spin chains within the layered honeycomb network with ordered moment of 0.22(1) μ_B/Ir site. Such a configuration sharply contrasts with the Néel or stripe states proposed in the Kitaev-Heisenberg model. The structure refinement reveals that the Ir atoms form nearly ideal 2D honeycomb lattice while the IrO_6 octahedra experience a trigonal distortion that is critical to the ground state. The results of this study provide much-needed experimental insights into the magnetic and crystal structure crucial to the understanding of the exotic magnetic order and possible topological characteristics in the 5*d*-electron based honeycomb lattice.

PACS numbers: 75.25.-j,61.05.cf,75.50.Ee

The 5*d*-based iridates have recently become a fertile yet largely uncharted ground for studies of new physics driven by the spin-orbit coupling (SOC). It is now recognized that the SOC (0.4 - 1 eV), which is proportional to Z^4 (Z is the atomic number), plays a critical role in the iridates, and rigorously competes with other relevant energies, particularly the on-site Coulomb interaction U (0.4 - 2.5 eV), which is significantly reduced because of the extended nature of the 5*d* orbitals. A new balance between the competing energies is therefore established in the iridates and drives exotic states seldom seen in other materials. Recent experimental observations and theoretical proposals for the iridates have already captured the intriguing physics driven by SOC: $J_{\text{eff}} = 1/2$ Mott state,[1–6] spin liquid in hyper-kagome structure,[7] high-T_C superconductivity,[8] Weyl semimetal with Fermi arcs,[9] correlated topological insulator with large gaps,[10,11] Kitaev mode,[12] 3D spin liquid with Fermionic spinons,[13] etc.

Of all iridates studied so far, Na_2IrO_3 has inspired a great deal of experimental and theoretical efforts.[11,14–18] In essence, the honeycomb lattice Na_2IrO_3 is predicted to be a topological insulator or a layered quantum spin Hall insulator.[10] However, conspicuous discrepancies among various theoretical proposals and experimental observations clearly point out a lack of much-needed characterization of the magnetic and crystal structures of Na_2IrO_3, whose band topology could vary significantly with slight variations in the crystal structure. This situation chiefly originates from the fact that the heavy transition metals such as Ir strongly absorb neutrons, which makes a comprehensive neutron study on the single crystal a nontrivial challenge.

In this paper, we report a combined neutron and x-ray diffraction study on relatively large, thin single-crystal Na_2IrO_3. This study reveals that Ir^{4+} ions order magnetically below 18.1(2) K, and form zigzag spin chains along the a axis of the honeycomb structure with an ordered moment of 0.22(1) μ_B/Ir. Moreover, the structural refinements illustrate that the Ir atoms feature a nearly perfect two-dimensional (2D) honeycomb lattice and a trigonal distortion characterized by the IrO_6 octahedra deviating from a high-symmetric cubic environment. These results are different from the previous x-ray powder diffraction study, where the honeycomb was characterized by three distinct bond lengths.[14]

Single crystals of Na_2IrO_3 were grown using a self-flux method from off-stoichiometric quantities of IrO_2 and Na_2CO_3. Similar technical details are described elsewhere.[4–6] The crystals have circular basal area corresponding to the honeycomb plane with diameters of $\sim$ 10 mm and thickness $\sim$ 0.1 mm. Such geometry provides a unique advantage to significantly alleviate the technical difficulty due to the inherent neutron absorption of the iridates. Energy dispersive x-ray spectroscopy (EDX) using a Hitachi/Oxford SEM/EDX indicates a perfect stoichiometry of Na_2IrO_3 throughout the crystals studied.

The x-ray diffraction measurements were performed using a Bruker SMART APEX CCD diffractometer with Mo K_α radiation and an Oxford cryostream cooler. More than 40 crystals from four different growth runs were screened at 125 K and full data sets were collected on four crystals. The neutron diffraction measurements were carried out at the HB1A triple axis spectrometer and HB3A four circle diffractometer at the High Flux Isotope Reactor at the Oak Ridge National Laboratory with fixed incident neutron wavelength of $\lambda = 2.367$ Å and 1.536 Å, respectively. For the HB1A diffraction measurement, the crystal is aligned in the $(0, k, l)$ scattering plane to allow the probing of various magnetic reflections.

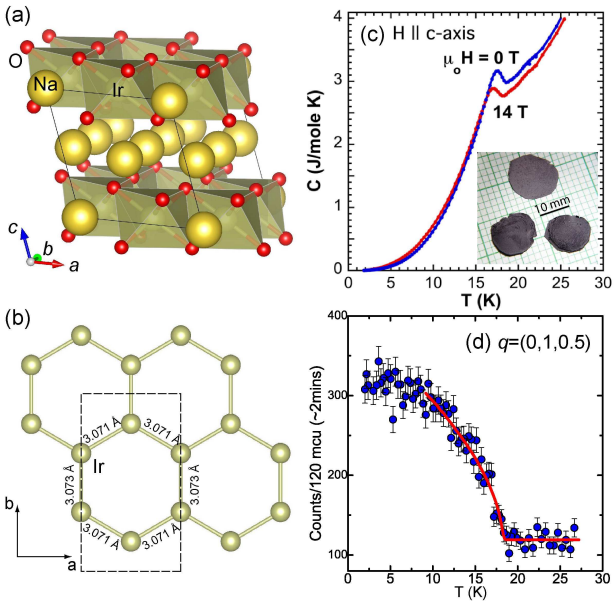

FIG. 1. (Color online) (a) Crystal structure of Na_2IrO_3 with $C2/m$ symmetry. (b) The honeycomb lattice formed by Ir atoms within the basal plane with nearly equivalent distance between neighboring Ir atoms. The dashed line denotes the unit cell. (c) Specific heat $C(T)$ at H = 0 and H = 14 T. Note that the application of a magnetic field of 14 Tesla suppresses the transition temperature by only 0.5 K, apparently not characteristic of a conventional Néel state. Inset shows the picture of single crystals used for diffraction experiments. (d) The T-dependence of peak intensity of the $(0, 1, 0.5)$ magnetic reflection from neutron diffraction measurement. The solid line is the power law fit described in the text.

The systematic absences in the single crystal x-ray diffraction measurements unambiguously determine that the space group of Na_2IrO_3 is $C2/m$ and not $C2/c$ as initially reported.[14] This finding is consistent with recent single crystal x-ray diffraction study by Choi *et al.* [Ref. 19]. The typical crystal diffraction pattern shows diffuse streaking, characteristic of stacking faults within the layer sequence. Stacking faults involving fractional translation and rotation of the fundamental $C2/m$ layer module have been modeled to some extent in the isostructural Li_2MnO_3.[20] Polytypism analogous to that observed in the micas is also possible. We adopted a structural model that allows for intermixing of the Na1 and Ir sites to artificially account for some amount of stacking disorder, yet retain the ideal stoichiometry. The overall structure exhibits a virtually regular honeycomb layer of edge-sharing IrO_6 octahedra, similar to that observed in other so-called dioctahedral sheets [e.g., gibbsite $Al(OH)_3$] in which the octahedra are slightly flattened perpendicular to layer stacking. In addition, the three O-Ir-O bond angles perpendicular to the basal plane are all greater than 90° whereas the bond angles across the shared edges are narrower, 84.1(3)° and 84.5(3)°, in contrast to the undistorted 90°, as shown in Fig. 2(a). The structural distortion indicates a presence of the trigonal crystal field in addition to the cubic crystal field, due to the repulsion of neighboring Ir atoms across the shared-edge of the octahedra. The trigonal crystal field in Na_2IrO_3 makes the otherwise well separated gap between $J_{eff} = 1/2$ and $3/2$ levels [Ref. 3] less pronounced, highlighting an important role in determining the electronic band structure topology.[21]

TABLE I. Structural parameters at T=125 K from single crystal x-ray diffraction measurements. The full data sets could be indexed using space group $C2/m$ with a = 5.319(1) Å, b = 9.215(2) Å, c = 5.536(1) Å, and β = 108.67(1)°. The Ir-O bond distances are 2.069(8), 2.067(9), and 2.060(12) Å, and the Ir···Ir distances are 3.073(1) and 3.0705(8) Å. Refinements are made using SHELXL-97,[22] yielding an agreement factor $R1 = 0.0687$ for 334 reflections with $F_{obs} > 4\sigma(F_{obs})$.

	Site	x	y	z	Occupancy	U(Å^2)
Ir1	4g	0	0.3332(1)	0	0.823(6)	0.006(1)
Na4	4g	0	0.3332(1)	0	0.177(6)	0.006(1)
Na1	2a	0	0	0	0.646(9)	0.014(2)
Ir2	2a	0	0	0	0.354(9)	0.014(2)
Na2	4h	0	0.8363	1/2	1	0.003(2)
Na3	2d	0	1/2	1/2	1	0.004(2)
O1	8j	0.259(3)	0.3294(7)	0.792(3)	1	0.001(3)
O2	4i	0.270(3)	0	0.792(3)	1	0.001(3)

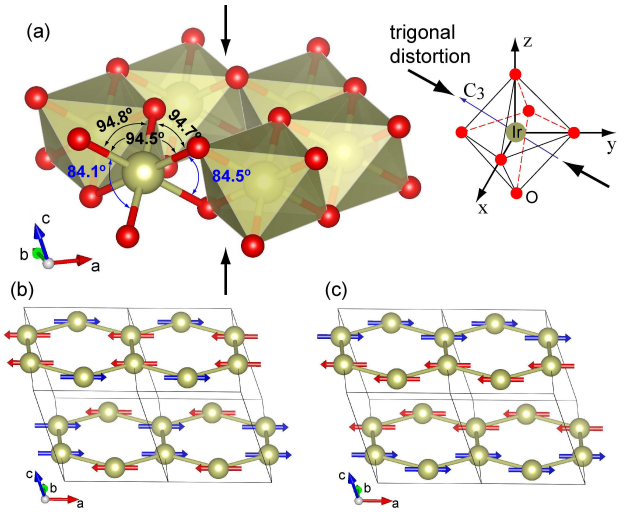

FIG. 2. (Color online) (a) Local structure within the basal plane. The compression of IrO_6 octahedron along the stacking leads to the decrease of O-Ir-O bond angles across the shared edges. (b)-(c) Comparison of stripe and zigzag order that are consistent with the symmetry associated with observed magnetic reflections. In both cases, the Ir moments between honeycomb layers are antiferromagnetically coupled.

The magnetic ground state is further characterized by the neutron diffraction on the single crystals. The magnetic propagation wave vector was determined to be $\mathbf{q}_m = (0, 1, 0.5)$ in the $C2/m$ notation based on exten-

sive survey in reciprocal space using the four-circle neutron diffractometer. Figure 1(d) shows that the magnetic Bragg peak intensity ($I_B \propto |M_s|^2$, M_s is the order parameter) disappears above $T_N = 18.1 \pm 0.2$ K, consistent with the anomaly observed in the specific heat data [Fig. 1(c)]. Fitting I_B to the power law scaling function of $(1 - T/T_N)^{2\beta}$ yields a critical exponent $\beta = 0.29(2)$ that is typical of a three-dimensional magnetic system. The determination of magnetic propagation wavevector and the correct description of the crystal structure put stringent constraints on the possible magnetic models. The magnetic reflection appearing at (0,1,0.5) rules out the Néel configuration [characterized by antiferromagnetically-coupled nearest neighboring spins with $\mathbf{q}'_m = (0, 0, 0.5)$] but leaves the choice of either stripe or zigzag order in the basal plane as depicted in Figs. 2(b)-2(c). Group theory analysis indicates that the magnetic representation $\Gamma_{\rm mag}$ can be decomposed into an irreducible representation (IR) $\Gamma_{\rm mag} = \Gamma_1 + \Gamma_2 + 2\Gamma_3 + 2\Gamma_4$ with corresponding basic vectors (BV) listed in Table II. Since the moment direction has been characterized to be along the a axis by magnetic susceptibility and polarized x-ray measurements,[15] this information is implemented to perform the model calculation and magnetic structural refinement. Figs. 3(a)-3(c) show the rocking scans of three characteristic magnetic Bragg reflections $\mathbf{q}_1 = (0, 1, 0.5)$, $\mathbf{q}_2 = (0, 3, 1.5)$ and $\mathbf{q}_3 = (0, 3, 0.5)$ in the $(0, k, l)$ scattering plane. The strongest reflection occurs at $\mathbf{q}_1$ and the intensity decrease sharply at $\mathbf{q}_2$ that has a larger momentum transfer. In contrast, there is no sign of magnetic scattering at $\mathbf{q}_3$ at base temperature. For single crystal magnetic scattering at wavevector transfer $\mathbf{q}$, the measured intensity follows

$$|F_\perp(\mathbf{q})|^2 = |\mathbf{F}_m(\mathbf{q})|^2 - [\hat{\mathbf{e}} \cdot \mathbf{F}_m(\mathbf{q})]^2. \qquad (1)$$

where $\hat{\mathbf{e}}$ is the unit vector along the $\mathbf{q}$, and $\mathbf{F}_m(\mathbf{q})$ is the magnetic structure factor that can be expressed as

$$\mathbf{F}_m(\mathbf{q}) = p \sum_{j=1}^{n} f_j(\mathbf{q}) \mathbf{S}_{\mathbf{k},j} \exp 2\pi i(\mathbf{q} \cdot \mathbf{r}_j). \qquad (2)$$

Here the sum is over all the magnetic atoms in the crystallographic cell, $p = r_e\gamma/2 = 0.2695$, $\mathbf{S}_{\mathbf{k},j}$ are the Fourier components proportional to the BVs listed in Table II, $\mathbf{r}$ is the vector position of atom j, and $f(\mathbf{q})$ is the magnetic form factor for the Ir^{4+} ions.[23]

As summarized in Table III, both stripe and zigzag spin orders give the identical ratio $|F_\perp(\mathbf{q}_2)/F_\perp(\mathbf{q}_1)|^2$. Therefore the magnetic scattering at these two reflections alone cannot distinguish the difference between the two spin configurations. However, the magnetic scattering at $\mathbf{q}_3$ is expected to be strong for the stripe spin configuration but absent for the zigzag spin chains; the absence of the magnetic scattering at $\mathbf{q}_3$ illustrated in Fig. 3(c) clearly indicates a presence of the zigzag spin order. To determine the magnitude of the magnetic moment/Ir, a large set of nuclear reflections under the same experimental configuration were collected to get the scale factor for normalization, yielding a magnetic moment of 0.22(1) μ_B/Ir; this is considerably smaller than that (1 μ_B/Ir) for a $S = 1/2$ system, consistent with early observations for systems such as Sr_2IrO_4 and $BaIrO_3$ where the ordered moment is no more than 15% of 1 μ_B/Ir.[4–6,24] The significantly reduced moment might be ascribed to the strong hybridization of the Ir $5d$ orbital with the ligand oxygen $2p$ orbital and the moments are largely canceled out in the antiferromagnetic state. Moreover, the wavevector scans presented in Figs. 3(d)-3(e) show resolution limited Gaussian profile and Lorentzian-like lineshape for the in-plane and out-of-plane magnetic correlation, respectively. The data reinforce that the spins form a long-range order in the honeycomb basal plane while a short range order might still remain to some extent (with correlation length $\xi \approx 139 \pm 21$ Å) between layers due to the inherent imperfection in crystal structure as suggested in the x-ray diffraction presented above.

In recent theoretical proposals, Na_2IrO_3 is regarded as one of a few model systems that can be mapped into the exactly solvable Kitaev model.[25] The combination of isotropic Heisenberg exchange interaction and anisotropic Kitaev term through strong spin-lattice coupling gives rise to a rich variety of low energy magnetic ground states. This includes the topologically nontrivial quantum spin Hall system in the weak interaction limit[10] and evolution from the conventional Néel order to the spin liquid state sandwiched by a stripe phase depending on the microscopic parameters in the strong spin-orbit coupling limit.[12,26] The geometric frustration due to the longer range exchange paths and the dynamic frustration caused by the Kitaev term leave the physical properties of Na_2IrO_3 highly tunable by small perturbations such as

TABLE II. Basis vectors (BVs) ψ_i of an IR of the space group $C2/m$ and $\mathbf{k} = (0, 1, 0.5)$. BVs are defined relative to the crystallographic axes. Magnetic moments for j atom in $l^{\rm th}$ cell are given by $\mathbf{m}_{l,j} = \sum_{\mathbf{k}} \mathbf{S}_{\mathbf{k},j} \exp(-2\pi i \mathbf{k} \cdot \mathbf{R}_\mathbf{l})$ and $\mathbf{S}_{\mathbf{k},j} = \sum_i C_i \psi_i$, where C_i is the mixing coefficient. Only Γ_3 and Γ_4 are relevant since they describe the correct spin direction along the a-axis.

	$\psi_1(\Gamma_1)$	$\psi_2(\Gamma_2)$	$\psi_3, \psi_4(\Gamma_3)$	$\psi_5, \psi_6(\Gamma_4)$
Ir $(0, 0.333, 0)$	(0,1,0)	(0,1,0)	(1,0,0),(0,0,1)	(1,0,0),(0,0,1)
Ir $(0, 0.667, 0)$	(0,1,0)	(0,-1,0)	(1,0,0),(0,0,1)	(-1,0,0),(0,0,-1)

TABLE III. Calculated magnetic scattering $|F_\perp(\mathbf{q}_i)|^2$ at $\mathbf{q}_1$ (normalized to 100), $\mathbf{q}_2$ and $\mathbf{q}_3$ for stripe and zigzag spin orders and their comparison to the measurement. Errorbar is statistical and refers to one standard deviation.

	$\mathbf{q}_1 = (0, 1, 0.5)$	$\mathbf{q}_2 = (0, 1, 1.5)$	$\mathbf{q}_3 = (0, 3, 0.5)$
Γ_3 (stripe)	100	51.1	186.5
Γ_4 (zigzag)	100	51.1	0.002
measurement	5.40 ± 0.38	2.77 ± 0.32	0

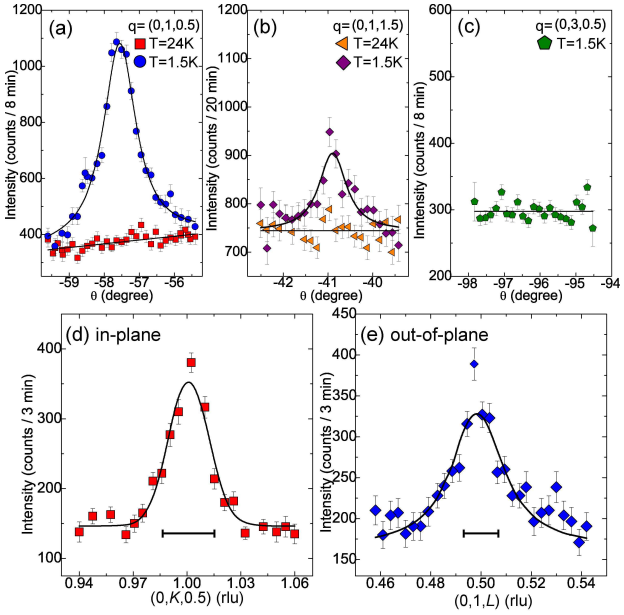

FIG. 3. (Color online) The rocking scans of characteristic magnetic reflections of (a) $(0, 1, 0.5)$, (b) $(0, 1, 1.5)$ and (c) $(0, 3, 0.5)$. (d)-(e) The in-plane and out-of-plane wavevector scans for the $(0, 1, 0.5)$ peak. Solid line in panel (e) is the fit to the Lorentzian form with instrument resolution convoluted. Horizontal bars in (d)-(e) denote the instrument resolution.

magnetic field, vacancies and structural distortions.[27–30] Only recently has the magnetic ground state been experimentally examined and proposed to be a possible zigzag spin state using resonant magnetic x-ray scattering.[15] The unexpected spin state inconsistent with the original Kitaev-Heisenberg model underscores the novelty of the magnetic ground state, prompting theoretical suggestions that the zigzag magnetic order could be explained only when the long-range magnetic Heisenberg interactions (J_2, J_3) [Refs. 16 and 27] or a trigonal distortion of the IrO_6 octahedra[31,32] in the $[1, 1, 1]$ direction (local basis of the octahedron) is taken into account. Indeed, a new quantum phase transition from normal to topological insulator is recently predicted in Na_2IrO_3 if both the long-range hopping and trigonal crystal field terms are included.[21] On the other hand, noticeable inconsistencies still exist in the band topology predictions that are likely due to the structural parameters used for the first-principles calculations.[10,33] With the presence of the trigonal crystal field, it is suggested that the $J_{\rm eff} = 1/2$ doublet is no longer as critical in Na_2IrO_3 as in Sr_2IrO_4,[1–5] $BaIrO_3$[6] and other layered iridates; instead, the trigonal crystal field (0.6 eV) and long-range hoping dictate the topological character, which is extremely sensitive to slight structural changes.[21]

One of the unique aspects of this work is that both neutron and x-ray diffraction data were collected from single crystals of Na_2IrO_3. The results of this work therefore provide the well-defined characteristics of the magnetic and crystal structures of the honeycomb lattice, and significantly improve our understanding of this intriguing system. We expect this study will help clarify the topological character of the ground state in Na_2IrO_3, a fertile ground yet to be fully explored.

We thank S. Okamoto and C. de la Cruz for invaluable discussions. Research at ORNL was sponsored in part by the Division of Chemical Sciences, Geosciences, and Biosciences, and the Scientific User Facilities Division, Office of Basic Energy Sciences, U.S. Department of Energy. The work at University of Kentucky was supported by NSF through grants DMR-0856234 and EPS-0814194.

[1] B. J. Kim *et al.*, Phys. Rev. Lett. **101**, 076402 (2008).
[2] S. J. Moon *et al.*, Phys. Rev. Lett. **101**, 226402 (2008).
[3] B. J. Kim *et al.*, Science **323**, 1329 (2009).
[4] M. Ge *et al.*, Phys. Rev. B **84**, 100402(R) (2011).
[5] S. Chikara *et al.*, Phys. Rev. B **80**, 140407(R) (2009).
[6] M. A. Laguna-Marco *et al.*, Phys. Rev. Lett. **105**, 216407 (2010).
[7] Y. Okamoto, M. Nohara, H. Aruga-Katori, and H. Takagi, Phys. Rev. Lett. **99**, 137207 (2007).
[8] F. Wang and T. Senthil, Phys. Rev. Lett. **106**, 136402 (2011).
[9] X. Wan, A. M. Turner, A. Vishwanath, and S. Y. Savrasov, Phys. Rev. B **83**, 205101 (2011).
[10] A. Shitade *et al.*, Phys. Rev. Lett. **102**, 256403 (2009).
[11] D. A. Pesin and L. Balents, Nat. Phys. **6**, 376 (2010).
[12] G. Jackeli and G. Khaliullin, Phys. Rev. Lett. **102**, 017205 (2009).
[13] Y. Zhou, P. A. Lee, T.-K. Ng, and F.-C. Zhang, Phys. Rev. Lett. **101**, 197201 (2008).
[14] Y. Singh and P. Gegenwart, Phys. Rev. B **82**, 064412 (2010).
[15] X. Liu *et al.*, Phys. Rev. B **83**, 220403(R) (2011).
[16] Y. Singh *et al.*, Phys. Rev. Lett. **108**, 127203 (2012).
[17] J. Reuther, R. Thomale, and S. Trebst, Phys. Rev. B **84**, 100406(R) (2011).
[18] Y. Yu and S. Qin, arXiv:1202.1610 (2012).
[19] S. Choi *et al.*, Phys. Rev. Lett. **108**, 127204 (2012).
[20] J. Bréger *et al.*, Journal of Solid Chemistry **178**, 2575 (2008).
[21] C. H. Kim, H. S. Kim, H. Jeong, H. Jin, and J. Yu, Phys. Rev. Lett. **108**, 106401 (2012).
[22] G. M. Sheldrick, Acta Cryst. **A64**, 112 (2008).
[23] K. Kobayashi, T. Nagao, and M. Ito, Acta Cryst A **67**, 473 (2011).
[24] G. Cao, J. Bolivar, S. McCall, J. E. Crow, and R. P. Guertin, Phys. Rev. B **57**, R11039 (1998).
[25] A. Kitaev, Ann. Phys. **321**, 2 (2006).
[26] J. Chaloupka, G. Jackeli, and G. Khaliullin, Phys. Rev. Lett. **105**, 027204 (2010).
[27] I. Kimchi and Y. Z. You, Phys. Rev. B **84**, 180407(R) (2011).
[28] H. C. Jiang, Z. C. Gu, X. L. Qi, and S. Trebst, Phys. Rev. B **83**, 245104 (2011).
[29] F. Trousselet, G. Khaliullin, and P. Horsch, Phys. Rev. B **84**, 054409 (2011).
[30] Y. Z. You, I. Kimchi, and A. Vishwanath, arXiv:1109.4155 (2011).
[31] S. Bhattacharjee, S. Lee, and Y. B. Kim, arXiv:1108.1806 (2011).
[32] B. J. Yang and Y. B. Kim, Phys. Rev. B **82**, 085111 (2010).
[33] H. Jin, H. Kim, H. Jeong, C. H. Kim, and J. Yu, arXiv:0907.0743 (2009).